All-angle negative refraction and imaging in a bulk medium made of metallic nanowires in the visible region

Yongmin Liu[1], Guy Bartal[1], Xiang Zhang[1,2,*]

*[1]NSF Nanoscale Science and Engineering Center (NSEC), 5130 Etcheverry Hall,
University of California, Berkeley, CA 94720-1740, USA
[2]Materials Sciences Division,Lawrence Berkeley National Laboratory,1 Cyclotron Road,
Berkeley, CA 94720, USA
[*]Corresponding author: xiang@berkeley.edu*

Abstract: We theoretically demonstrated that all-angle negative refraction and imaging can be implemented by metallic nanowires embedded in a dielectric matrix. When the separation between the nanowires is much smaller than the incident wavelength, these structures can be characterized as indefinite media, whose effective permittivities perpendicular and parallel to the wires are opposite in signs. Under this condition, the dispersion diagram is hyperbolic for transverse magnetic waves propagating in the nanowire system, thereby exhibiting all-angle negative refraction. Such indefinite media can operate over a broad frequency range (visible to near-infrared) far from any resonances, thus they offer an effective way to manipulate light propagation in bulk media with low losses, allowing potential applications in photonic devices.

©2008 Optical Society of America

References and links

1. V. G. Veselago, "The electromagnetics of substances with simultaneously negative ε and μ," Sov. Phys. Usp. **10**, 509-514 (1968).
2. J. B. Pendry, "Negative refraction makes a perfect lens," Phys. Rev. Lett. **85**, 3966-3969 (2000).
3. N. Fang, H. Lee, C. Sun, and X. Zhang, "Sub–diffraction-limited optical imaging with a silver superlens," Science **308**, 534-537 (2005).
4. Xiang Zhang and Zhaowei Liu, "Superlenses to overcome the diffraction limit," Nat. Mater. **7**, 435, (2008)
5. R. A. Shelby, D. R. Smith, and S. Schultz, "Experimental verification of a negative index of refraction," Science **292**, 77-79 (2001).
6. C. G. Parazzoli, R. B. Greegor, K. Li, B. E. C. Koltenbah, and M. Tanielian, "Experimental verification and simulation of negative index of refraction using Snell's law," Phys. Rev. Lett. **90**, 107401 (2003).
7. A. A. Houck, J. B. Brock, and I. L. Chuang, "Experimental observations of a left-handed material that obeys Snell's law," Phys. Rev. Lett. **90**, 137401 (2003).
8. M. Notomi, "Theory of light propagation in strongly modulated photonic crystals: Refractionlike behavior in the vicinity of the photonic band gap," Phys. Rev. B **62**, 10696-10705 (2000).
9. C. Luo, S. G. Johnson, J. D. Joannopoulos, and J. B. Pendry, "Negative refraction without negative index in metallic photonic crystals," Opt. Express **11**, 745-754 (2003).
10. X. H. Hu and C. T. Chan, "Photonic crystals with silver nanowires as a near-infrared superlens," Appl. Phys. Lett. **85**, 1520-1522 (2004).
11. E. Cubukcu, K. Aydin, E. Ozbay, S. Foteinopoulou, and C. M. Soukoulis, "Negative refraction by photonic crystals," Nature **423**, 604-605 (2003).
12. P. V. Parimi, W. T. Lu, P. Vodo, and S. Sridhar, "Photonic crystals: Imaging by flat lens using negative refraction," Nature **426**, 404 (2003).
13. S. Foteinopoulou and C. M. Soukoulis, "Negative refraction and left-handed behavior in two-dimensional photonic crystals," Phys. Rev. B **67**, 235107 (2003).
14. A. Berrier, M. Mulot, M. Swillo, M. Qiu, L. Thylen, A. Talneau, and S. Anand, "Negative refraction at infrared wavelengths in a two-dimensional photonic crystal," Phys. Rev. Lett. **93**, 073902 (2004).
15. Schonbrun, Q. Wu, W. Park, T Yamashita, C. J. Summers, M. Abashin and Y. Fainman, "Wave front evolution of negatively refracted waves in a photonic crystal", Appl. Phys. Lett. **90**, 041113 (2007).
16. C. M. Soukoulis, S. Linden and M. Wegener, "Negative refractive index at optical wavelengths," Science **315**, 47-49 (2007).

17. M. I. Stockman, "Criterion for negative refraction with low optical losses from a fundamental principle of causality," Phys. Rev. Lett. **98**, 177404 (2007).
18. G. Dolling, W. Wegener, C. M. Soukoulis and S. Linden, "Negative-index metamaterial at 780 nm wavelength," Opt. Lett. **32**, 53-55 (2007).
19. N. Liu, H. C. Guo, L. W. Fu, S. Kaiser, H. Schweizer, and H. Giessen, "Three-dimensional photonic metamaterials at optical frequencies," Nat. Mater. **7**, 31-37 (2008).
20. H. Shin and S. H. Fan, "All-angle negative refraction for surface plasmon waves using a metal-dielectric-metal structure," Phys. Rev. Lett. **96**, 073907 (2006).
21. H. J. Lezec, J. A. Dionne, and H. A. Atwater, "Negative refraction at visible frequencies," Science **316**, 430-432 (2007).
22. M. Scalora, G. D'Aguanno, N. Mattiucci, M. J. Bloemer, D. de Ceglia, M. Centini, A. Mandatori, C. Sibilia, N. Akozbek, M. G. Cappeddu, M. Fowler, and Joseph W. Haus, "Negative refraction and sub-wavelength focusing in the visible range using transparent metallo-dielectric stacks," Opt. Express **15**, 508-523 (2007).
23. X.B. Fan, G. P. Wang, J. C. W. Lee and C. T. Chan, "All-angle broadband negative refraction of metal waveguide arrays in the visible range: theoretical analysis and numerical demonstration," Phys. Rev. Lett. **97**, 073901 (2007).
24. B. Wood, J. B. Pendry, and D. P. Tsai, "Directed subwavelength imaging using a layered metal-dielectric system," Phys. Rev. B **74**, 115116 (2006).
25. A. J. Hoffman, L. Alekseyev, S. S. Howard, K. J. Franz, D. Wasserman, V. A. Podolskiy, E. E. Narimanov, D. L. Sivco, and C. Gmachl " Negative refraction in semiconductor metamaterials," Nat. Mater. **6**, 946-950 (2007).
26. A. Salandrino and N. Engheta, "Far-field subdiffraction optical microscopy using metamaterial crystals: theory and simulations," Phys. Rev. B **74**, 075103 (2006).
27. Z. Jacob, L. V. Alekseyev, and E. Narimanov, "Optical Hyperlens: Far-field imaging beyond the diffraction limit," Opt. Express **14**, 8247-8256 (2006).
28. Zhaowei Liu, Hyesog Lee, Yi Xiong, Cheng Sun, and Xiang Zhang, "Far-field optical hyperlens magnifying sub-diffraction-limited objects," Science **315**, 1686 (2007).
29. I. I. Smolyaninov, Y. J. Hung, and C. C. Davis, "Magnifying Superlens in the Visible Frequency Range," Science **315**, 1699-1701 (2007).
30. D. R. Smith and D. Schurig, "Electromagnetic wave propagation in media with indefinite permittivity and permeability tensors," Phys. Rev. Lett. **90**, 077405 (2003).
31. H. Masuda and K. Fukuda, "Ordered metal nanohole arrays made by a two-step replication of honeycomb structures of anodic alumina," Science **268**, 1466-1468 (1995).
32. C. R. Martin, "Nanomaterials: a membrane-based synthetic approach," Science **266**, 1961-1966 (1994).
33. J. Elser, V. A. Podolskiy, I. Salakhutdinov, and E. E. Narimanov, "Nanowire metamaterials with extreme optical anisotropy," Appl. Phys. Lett. **89**, 261102 (2006).
34. A. Sihvola, Electromagnetic Mixing Formulas and Applications, Institution of Electrical Engineers (1999).
35. C. A. Foss, G. L. Hornyak, J. A. Stockert, and C. R. Martin, "Template synthesized nanoscopic gold particles: optical spectra and the effects of particle size and shape," J. Phys. Chem. **98**, 2963-2971 (1994).
36. P. B. Johnson, R. W. Christy, "Optical constants of the noble metals," Phys. Rev. B **6**, 4370-4379 (1972).
37. H. Raether, Surface Plasmons: On Smooth and Rough Surfaces and on Gratings, Springer, Berlin (1988).
38. This is valid for $k_x < \pi/d$, where d is the average distance between wires. The cutoff is at $k_x < \pi/d >> 2\pi/\lambda_0$.
39. P. A. Belov, "Backward waves and negative refraction in uniaxial dielectrics with negative dielectric permittivity along the anisotropy axis," Microwave Opt. Technol. Lett. **37**, 259-263 (2003).
40. V. A. Podolskiy and E. E. Narimanov, "Strongly anisotropic waveguide as a nonmagnetic left-handed system," Phys. Rev. B **71** 201101(R) (2005).
41. T. Dumelow, J. A. P. da Costa, and V. N. Freire, "Slab lenses from simple anisotropic media," Phys. Rev. B **72**, 235115 (2005).
42. G. Shvets, S. Trendafilov, J. B. Pendry, and A. Sarychev, "Guiding, focusing, and sensing on the subwavelength scale using metallic wire arrays," Phys. Rev. Lett. **99**, 053909 (2007).
43. P. Ikonen, C. Simovski, S. Tretyakov, P. Belov, and Y. Hao, "Magnification of subwavelength field distributions at microwave frequencies using a wire medium slab operating in the canalization regime," Appl. Phys. Lett. **91**, 104102 (2007).

1. Introduction

Negative refraction and superlensing have been extensively studied in negative-index metamaterials (NIMs) and photonic crystals (PCs) [1-15]. Veselago theoretically predicted that at the interface of a positive-index material and a negative-index material, the Snell's law is reversed [1]. Pendry has further extended this concept, showing that a flat slab of NIMs can make a perfect lens for sub-diffraction-limited imaging [2]. Such a superlens has been implemented by a silver film with the properly designed thickness and working wavelength [3,4]. Both negative refraction and imaging effects have been observed in the microwave region based on artificial NIMs, where the electric permittivity and magnetic permeability are simultaneously negative [5-7]. Researchers have also explored similar novel phenomena by

engineering the dispersion of photonic bands in dielectric and metallic PCs [8-15], proving that negative refraction can exist without a negative refractive index.

So far, demonstration of negative refraction and imaging in bulk materials at visible frequencies still remains very challenging [16-19]. As NIMs rely on resonance, they are usually accompanied by significant losses, especially in the visible region. Moreover, the feature size of NIMs, as well as the period of PCs should be controlled at nanometer precision within the entire bulk volume. Very recently, people have investigated negative refraction of surface plasmon polaritons (SPPs) at visible frequencies, arising from the anomalous dispersion of SPPs in specific frequency range in planar plasmonic waveguide structures [20,21]. Negative refraction and imaging at visible frequencies were also proposed in metal-dielectric multilayers [22-24], whereas an indirect observation of negative refraction in mid-infrared region was reported in a semiconductor multilayer structure with the total thickness about one wavelength [25]. Using curved metal-dielectric multilayers, researchers have demonstrated the far-field magnifying hyperlens [26-29].

In the long-wavelength limit, the metal-dielectric multilayer structure in refs. [22-29] can be described as indefinite materials, where the transverse and longitudinal effective permittivities are different in signs as introduced by Smith and Schruig [30]. In this paper we study and design a bulk indefinite material composed of aligned arrays of metallic nanowires in a dielectric matrix, to implement all-angle negative refraction over a broad band in the optical frequency region. Such negative diffraction is not sensitive to the azimuthal angle, nanowire arrangement or geometry imperfection. More importantly, these structures can operate far from any resonances. Therefore the material loss is significantly lower than negative-index materials and plasmonic structures at visible frequencies [18,20,21], allowing much longer propagation distances. Our analyses, based on the dynamical Maxwell-Garnet theory, are in good agreements with finite-element simulations considering the actual nanowire structure and material property.

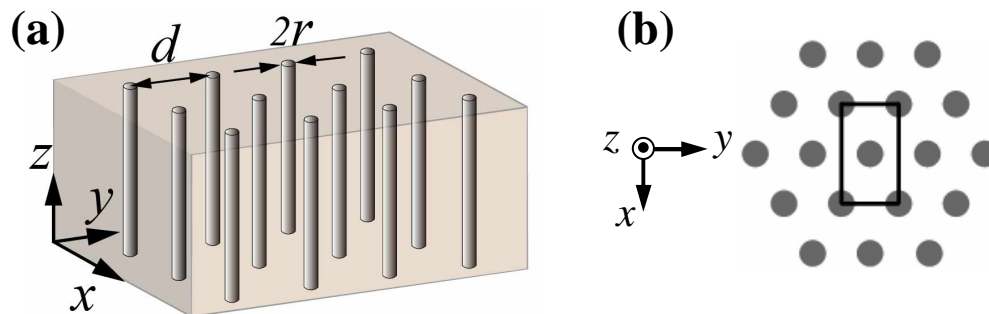## 2. Effective material properties of metallic nanowires

Fig. 1. (a). Schematic of metallic nanowires embedded in a dielectric matrix. (b) Illustration of the hexagonal lattice of nanowires fabricated by an anodized alumina template. The rectangular unit cell is adopted in the finite-element simulations.

Figure 1(a) schematically illustrates the structure of metallic nanowires embedded in a dielectric host. This structure can be fabricated by electrochemically growing metallic nanowires in a porous alumina template, which is prepared by the anodization method in a self-organized way [31]. Such a method has proved to be a low-cost and high-yield technique for fabricating different kinds of nanostructures including nanowires, nanodots and nanotubes [32].

When the geometric parameters, i.e., the wire radius (r) and the distance between two neighboring wires (d), are much smaller than the free space wavelength (λ_0) of the incident electromagnetic wave, the underlying system can be considered as an effective uniaxial

medium [33, 34]. We utilize the dynamical Maxwell-Garnett theory to determine the permittivity parallel to wires ($\varepsilon_{//}$) and perpendicular to wires ($\varepsilon_{\perp}$), which are given by the following equations [34, 35]:

$$\varepsilon_{//} = p\varepsilon_m + (1-p)\varepsilon_d \qquad (1a)$$

$$\varepsilon_{\perp} = \varepsilon_d + \frac{p\varepsilon_d(\varepsilon_m - \varepsilon_d)}{\varepsilon_d + (1-p)(\varepsilon_m - \varepsilon_d)q_{eff}} \qquad (1b)$$

Here p is the filling ratio of metal, ε_m and ε_d are the permittivity of metal and dielectric, respectively. In Eq. (1b), the effective depolarization factor perpendicular to nanowires is defined as

$$q_{eff} = \frac{1}{2} - \frac{1}{3}(\frac{2\pi}{\lambda_0} \cdot r)^2 - \frac{2}{9}(\frac{2\pi}{\lambda_0} \cdot r)^3 \cdot i \qquad (2)$$

The first term on the right-handed site of Eq. (2) is the Lorentz depolarizing factor perpendicular to the nanowire at the long wavelength limit. The second term is the dynamical depolarization when the nanowire radius is not so small comparing to the incident wavelength. The third term accounts for damping of the induced dipole due to radiation emission. In the Cartesian coordinate shown in Fig. 1(a), one can see that $\varepsilon_x = \varepsilon_y = \varepsilon_{\perp}$ and $\varepsilon_z = \varepsilon_{//}$.

In this paper, we focus on silver nanowires as the material loss in the visible region is smallest among the noble metals. The permittivity of silver is described by the Drude model $\varepsilon_m(\omega) = \varepsilon_{\infty} - \frac{\omega_p^2}{\omega(\omega + i\gamma_c)}$, where the high-frequency bulk permittivity $\varepsilon_{\infty} = 6$, the bulk plasmon frequency $\omega_p = 1.5 \times 10^{16} \, rad/s$, and the collision frequency $\gamma_c = 7.73 \times 10^{13} \, rad/s$ are obtained by fitting the model to the experimental data from the literature [36]. Alumina (Al$_2$O$_3$) is the dielectric matrix with permittivity $\varepsilon_d = 2.4$ for the entire frequency region of our interest [35].

Figure 2 depicts the effective permittivities of metallic nanowires for the filling ratios $p = 0.227$ and $p = 0.325$ at the long wavelength limit ($q_{eff} = 1/2$). It can be seen that the real part of $\varepsilon_{//}$ continuously changes from negative to positive as the wavelength decreases. In contrast, $\varepsilon_{\perp}$ has a resonant behavior (due to localized SPPs) accompanied by a strong dispersion and a very large imaginary part [37]. When increasing the filling ratio, the critical frequency at which $Re(\varepsilon_{//}) = 0$ shift to shorter wavelengths, while the resonance for $\varepsilon_{\perp}$ has a red shift to longer wavelengths. In general, there is a very broad spectral region (from visible to infrared) satisfying $\varepsilon_{//} \cdot \varepsilon_{\perp} < 0$, which is critical for negative refraction and imaging as discussed in the following text.
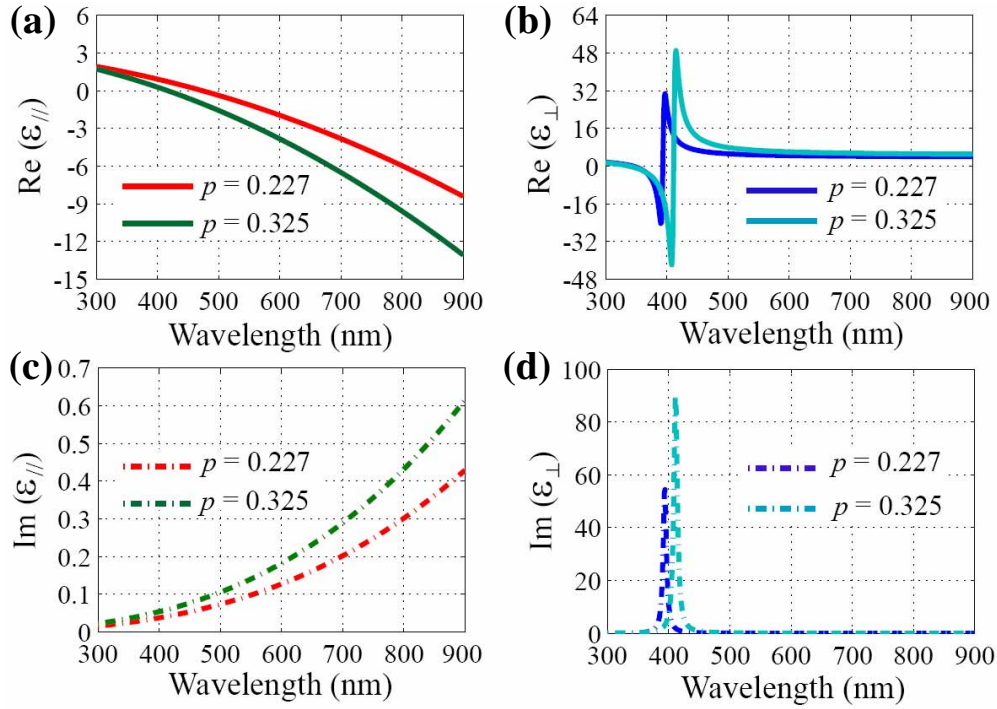
Fig. 2. Effective permittivities for silver nanowires embedded in an alumina matrix with two different filling ratios. (a) and (b) plot the real part of the permittivity parallel and perpendicular to the nanowire, respectively. (c) and (d) are the corresponding imaginary parts.

3. General theory of all-angle negative refraction by indefinite media

Now let us consider the electromagnetic (EM) wave propagation in a nonmagnetic uniaxial material with the electric permittivity tensor given by

$$\ddot{\varepsilon} = \varepsilon_0 \begin{pmatrix} \varepsilon_x & 0 & 0 \\ 0 & \varepsilon_y & 0 \\ 0 & 0 & \varepsilon_z \end{pmatrix}. \tag{3}$$

The general format for the electric field and magnetic field of a plane wave with frequency ω and wave vector $\vec{k}$ can be written as

$$\vec{E} = \vec{E}_0 e^{i(\vec{k}\cdot\vec{r}-\omega t)}, \tag{4}$$

$$\vec{H} = \vec{H}_0 e^{i(\vec{k}\cdot\vec{r}-\omega t)}. \tag{5}$$

In the principle axis, suppose the wave vector $\vec{k}$ lies in the x-z plane. From Maxwell's equations $\nabla \times \vec{E} = -\frac{\partial \vec{B}}{\partial t}$ and $\nabla \times \vec{H} = \frac{\partial \vec{D}}{\partial t} = \frac{\partial(\ddot{\varepsilon}\cdot\vec{E})}{\partial t}$, a transverse magnetic wave, which satisfies the condition of $\vec{k}\cdot\vec{H}=0$, can be expressed explicitly as

$$\vec{H} = H_0 \hat{e}_y \exp[i(k_x x + k_z z - \omega t)], \tag{6}$$

$$\vec{E} = \frac{H_0}{\omega \varepsilon_0}(\frac{k_z}{\varepsilon_x}\hat{e}_x - \frac{k_x}{\varepsilon_z}\hat{e}_z)\exp[i(k_x x + k_z z - \omega t)]. \tag{7}$$

Here $\hat{e}_x$, $\hat{e}_y$ and $\hat{e}_z$ are the unit vectors along the x, y and z axis, respectively. Consequently, the time-averaged Poynting vector for TM waves is readily obtained

$$< \bar{S} >= \frac{1}{2}\bar{E}\times\bar{H}^* = \frac{\bar{\varepsilon}\cdot\bar{k}}{2\omega\varepsilon_0\varepsilon_x\varepsilon_z}H_0^2. \tag{8}$$

From Maxwell's equations, the dispersion relation for TM waves is given by

$$\frac{k_x^2}{\varepsilon_z}+\frac{k_z^2}{\varepsilon_x}=\frac{\omega^2}{c^2}, \tag{9}$$

where c is the light velocity in vacuum. In particular, we study the case of $\varepsilon_x > 0$ and $\varepsilon_z < 0$, representing an "indefinite material" as introduced by Smith and Schruig [30]. Under this condition, the equifrequency contour of the medium is hyperbolic in the (k_x, k_z) plane (see Fig. 3(a)). Namely, any real k_x has a real solution for k_z, indicating that the wave can propagate without any cutoff [38]. This is to say, such materials support propagation of waves with large wave vectors (*i.e.*, with $k_x > 2\pi/\lambda_0$), which are initially evanescent in free space [30].
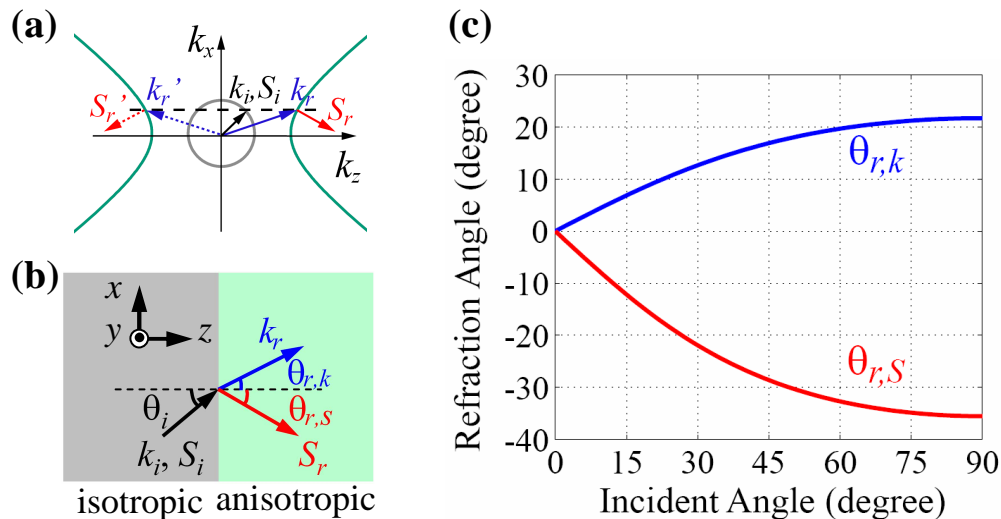

Fig. 3. (a). The equifrequency contour of an indefinite material with $\varepsilon_x = 4.515$ and $\varepsilon_z = -2.530$ (green hyperbola), as well as the equifrequency contour of an isotropic material (gray circle). The refracted wave vector (solid blue arrow) and Poynting vector (solid red arrow) can be determined by satisfying the causality theorem and the conservation of the tangential wave vector. While the other set of refracted wave vector (dotted blue arrow) and Poynting vector (dotted red arrow) are physically incorrect. (b) Schematic diagram of negative refraction for a TM wave, which is incident from an isotropic material to an indefinite one with $\varepsilon_x > 0$ and $\varepsilon_z < 0$. (c) Refracted angles for the wave vector (blue) and Poynting vector (red) at various incident angles. Note the Poynting vector undergoes negative refraction for all incident angles.

Consider a TM polarized light incident from a normal isotropic material, in which the wave vector and Poynting vector are parallel, to an indefinite medium with $\varepsilon_x > 0$ and $\varepsilon_z < 0$ (Figs. 3(a) and 3(b)). At the interface, there are two solutions (presented by solid and dashed blue arrows in Fig. 3(a)) satisfying the continuity of the tangential component of $\bar{k}$ (that is, k_x). However, according to the causality principle [5-15], the energy must flow away from

the interface, *i.e.*, $S_z = \hat{e}_z \cdot \bar{S} > 0$. It can be readily shown from Eq. (8), that for positive ε_x only the solution represented by the solid blue arrow in Fig. 3(a) satisfies the condition

$$S_z = \frac{\hat{e}_z \cdot \bar{k}}{\varepsilon_x} \frac{H_0^2}{2\omega\varepsilon_0} > 0 .$$ (10)

The tangential component of $\bar{S}$ is written as

$$S_x = \frac{k_x}{\varepsilon_z} \frac{H_0^2}{2\omega\varepsilon_0} .$$ (11)

Since ε_z is negative and k_x is continuous, the sign of S_x flips at the interface. This gives rise to negative refraction at the interface as shown in Fig. 3(b), which was also discussed in reference [39]. In fact, we find that the *x*-component of the group velocity is negative, which results in negative refraction in this nanowire composite (or so-called negative group-index).

We can quantitively determine the refraction angles for the wave vector and Poynting vector defined as

$$\theta_{r,k} = \tan^{-1}(\frac{k_x}{k_z}) ,$$ (12a)

$$\theta_{r,S} = \tan^{-1}(\frac{S_x}{S_z}) = \tan^{-1}(\frac{k_x / \varepsilon_z}{k_z / \varepsilon_x}) ,$$ (12b)

respectively. Figure 3(c) plots the numerical calculation based on Eqs. (9) and (12) when $\varepsilon_x =$ 4.515 and $\varepsilon_z = -2.530$ (corresponding to real parts of ε_x and ε_z for nanowires with the filling ratio $p = 0.227$ at 632.8nm wavelength). One can see that the refraction angle of the Poynting vector is always negative for any incident angle while the phase front always propagates in the positive direction. Moreover, it should be noted that the angle between the Poynting vector and wave vector is acute, namely

$$\phi = \cos^{-1}(\frac{\bar{k} \cdot \bar{S}}{|\bar{k}| \cdot |\bar{S}|}) = \cos^{-1}(\frac{\omega^2 / c^2}{\sqrt{k_x^2 + k_z^2} \sqrt{(k_x / \varepsilon_z)^2 + (k_z / \varepsilon_x)^2}}) .$$ (13)

This is in contrast to NIMs, where the Poynting vector and wave vector are anti-parallel.

4. Numerical simulations and discussions

The aforementioned analyses of negative refraction are confirmed by full-wave simulations, which take into account the actual nanowire structure and material property. Using COMSOL Multiphysics ^{TM}3.4, a commercial electromagnetic solver based on the finite element method (FEM), we numerically demonstrate negative refraction and imaging of TM waves by metallic nanowires at visible frequencies. In the simulation, the distance between two neighboring nanowires is set to 110nm and the nanowire radius is 27.5nm (corresponding to the filling ratio $p = 2\pi \cdot r^2/(\sqrt{3} \cdot d^2) = 0.227$). The rectangular unit cell shown in Fig. 1(b) is adopted in the simulation. Periodic boundary conditions are applied along the *y*-axis, and matched boundary conditions are along the *x*- and *z*-axes. A transverse magnetic (magnetic field is polarized along the *y*-axis) Gaussian beam with a 2μm width is incident at 30 degrees on 1.5μm-long nanowire arrays.

Figures 4(a) and 4(b) plot the cross-sectional view of the absolute electric field and time-averaged Poynting vector (energy flow) in the *x*-*z* plane, respectively, at the excitation wavelength of 632.8nm. The results evidently show negative refraction at the interfaces, with refraction angle of about -22 degrees, in a good agreement with the analytical prediction based on the dynamical Maxwell-Garnett theory (see Fig. 3(c)). It is noted that the field intensity is enhanced in the gap between nanowires, arising from the existence of SPPs [37]. We also

perform finite element simulation replacing the nanowire structure with a homogenous slab with effective permittivities $\varepsilon_x = 4.515 + 0.056i$ and $\varepsilon_z = -2.530 + 0.149i$, calculated from Eqs. (1) and (2) according to the dynamical Maxwell-Garnett theory. Once again, the excellent agreement between Figs. 4(a) and 4(c), as well as Figs. 4(b) and 4(d) prove the validity of the effective media approximation for any beams incident from free space to the underlying indefinite medium.
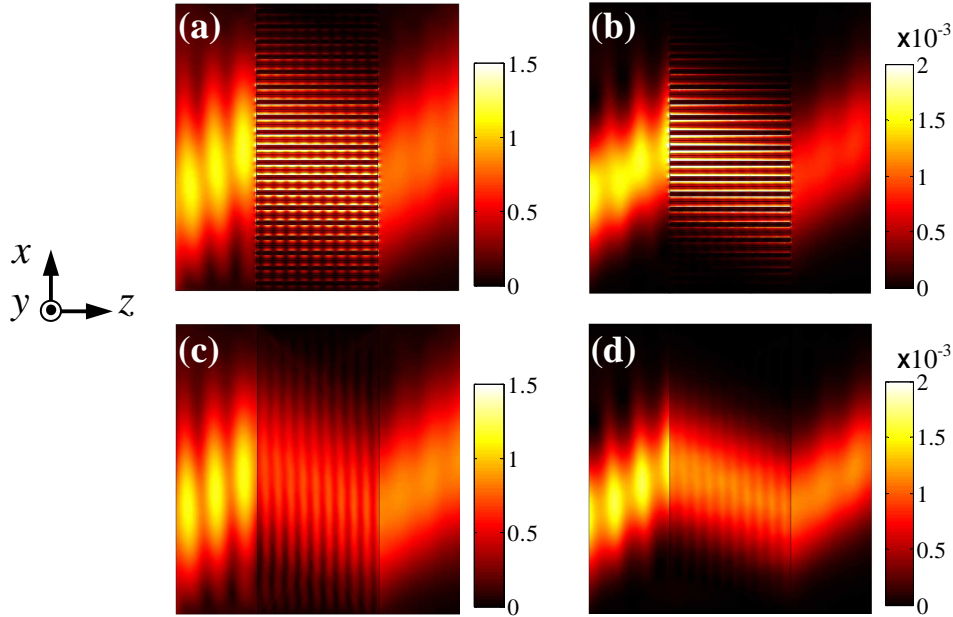

Fig. 4. Finite-element simulations showing negative refraction by metallic nanowire structures at 632.8nm wavelength. Figs. (a) and (c) plot the absolute value of the electric field, and Figs. (b) and (d) plot the time-averaged Poynting vector. The 3D full-wave simulations ((a) and (b)) considering the real nanowire structure agree very well with the simulation based on the effective medium approximation ((c) and (d)). In the simulations of (a) and (c), the nanowires are arranged in a hexagonal lattice as shown in Fig. 1(b), the radius of nanowires is 27.5nm, and the separation between adjacent wires is 110nm. Those parameters are kept same for simulations shown in Figs. 5-6.

One of the most attractive advantages to implement negative refraction by nanowires is that the loss can be significantly reduced, compared to NIMs [18] or plasmonic structures with anomalous dispersion [20, 21] at visible frequencies. At frequencies far away from the resonance of $\varepsilon_\perp$, the system is intrinsically low-loss. For example, at 632.8nm wavelength with the filling ratio $p = 0.227$, the intensity of the refracted light only attenuates to 77% after propagating one micrometer. This indicates a loss that is a few orders of magnitudes lower than other structures at visible wavelengths [18, 20, 21]. At longer wavelength, the smaller penetration depth of the field into metal gives rise to even less Ohmic losses. Consequently, the transmission efficiency of light in the nanowire metamaterials can be further improved. Moreover, in contrast to photonic crystals [7-14], the negative refraction is much more tolerant to the deviation of nanowire geometry and lattice, as long as the effective media approximation is valid. For simplicity, the simulations in this paper consider an ideal hexagonal lattice of nanowires. But in reality, the nanowires can be disordered, and still maintain negative refraction, if the spacing between them is much smaller than the wavelength.

Interestingly, while such indefinite materials exhibit negative refraction (related to the direction of Poynting vector) the phase propagation (associated with the wave-vector) still remains positive. The refraction properties of nanowires depend on the orientation of the optical axis with respect to the surface normal. As such, plane wave propagation in a prism-shaped indefinite material will not always result in negative refraction, as shown in NIMs or PCs [5-7, 13]. This is demonstrated in Fig. 5, where TM wave propagation through a prism-shaped sample is simulated. Clearly, a horizontally incident wave is refracted from the 15-degree angle facet in a positive way, seemingly contradictive to the results shown in Figs. 4(a)-4(d). However, this could be explained considering the ray optics based on the equifrequncy contour, which is illustrated in Fig. 5(b). Since the continuity of the tangential wave vector along the interface and causality principle should be satisfied, positive refraction takes places at the exit surface of the prism.
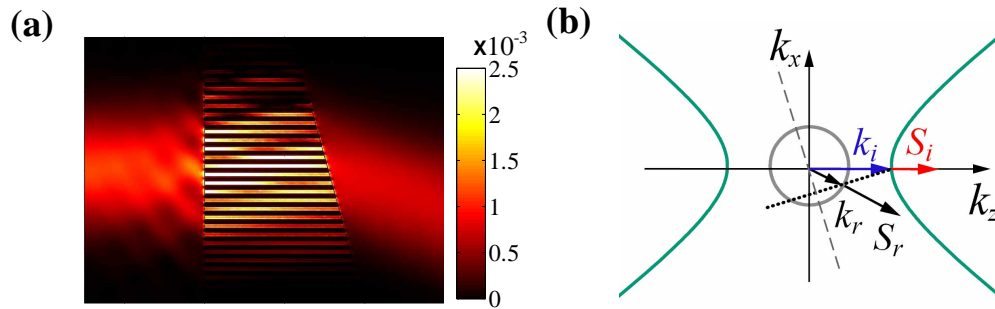

Fig. 5. (a). The time-averaged Poynting vector for a TM wave transmitted through a prism-shaped nanowire slab. The surface normal of the prism has a 15-degree angle with respect to the z-axis. Positive refraction takes place at the exit surface. (b). Interpretation of the refraction behavior at the exit surface based on the equifrequency contour.

Finally, we also show that a flat slab made of indefinite materials can be used for imaging, as presented by the ray diagram in Fig. 6(a). The full-wave simulation of the imaging effect by nanowire arrays is shown in Fig. 6(b), at the wavelength of 632.8nm for a source located 0.5μm in front of a 2.0μm-thick nanowire slab. An elongated focus point is formed after the nanowire lens. The aberration of the imaging results from the fact that the effective refraction index of the indefinite material is angle-dependent [41]. By adjusting the geometry of nanowires, subwavelength and magnified imaging can be achieved [42, 43].
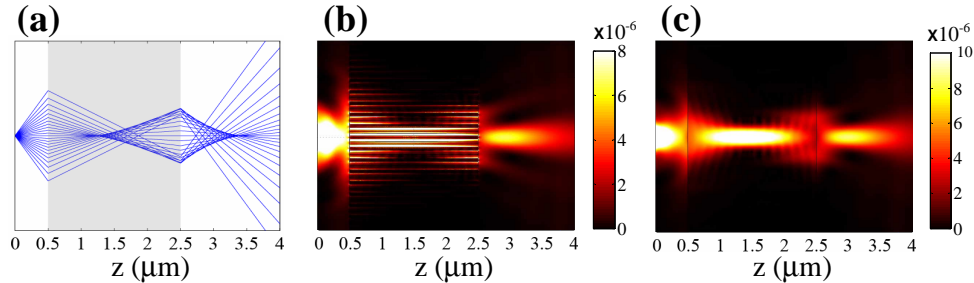

Fig. 6. (a). Ray optics showing that an indefinite-material slab is able to form partial imaging inside and outside the slab. The source is placed 500nm in front the slab. The gray region represents a 2μm-thick indefinite slab with $\varepsilon_x = 4.515$ and $\varepsilon_z = -2.530$. (b) The time-averaged Poynting vector in the 3D finite-element simulation. (c) Same as (b), but the realistic nanowire structure in (b) is replaced by a homogeneous indefinite material with effective permittivies calculated from the dynamical Maxwell-Garnett theory.

5. Conclusions

To summarize, we have deigned a bulk indefinite metamaterial using metallic nanowires to realize all-angle negative refraction and imaging in the visible region. Finite-element simulations taking into account the actual structure and material property agree very well with the analyses based on the dynamical Maxwell-Garnet theory. The negative refraction, arising from the hyperbolic equifrequency contour of the system, is fundamentally different from what have been observed in negative-index materials and photonic crystals. It is intrinsically low-loss and broad-band, because the mechanism does not rely on any resonances. Moreover, our approach is insensitive to the variation of wire diameters and separations between wires, under the effective media approximation at the long wavelength limit. We expect those intriguing phenomena to stimulate experimental efforts towards imaging, wave guiding and light manipulation in three dimensions over a very broad frequency band.